Available online at www.sciencedirect.com
ScienceDirect
Journal of Power Sources 162 (2006) 992–1002
JOURNAL OF POWER SOURCES
www.elsevier.com/locate/jpowsour

Three-dimensional, two-phase, CFD model for the design of a direct methanol fuel cell

Valeri A. Danilov [a], Jongkoo Lim [a], Il Moon [a,*], Hyuk Chang [b]

[a] *Department of Chemical Engineering, Yonsei University Seodaemun-gu Shinchon-dong 134, Seoul 120-749, South Korea*
[b] *Samsung Advanced Institute of Technology, Suwon 440-600, South Korea*

Received 11 April 2006; accepted 26 July 2006
Available online 18 September 2006

Abstract

This study presents a computational fluid dynamics (CFD) model for modelling gas evolution and current distribution in a direct methanol fuel cell (DMFC). The improved two-phase model includes a new sub-model for estimating the interface mass transfer without empirical correlations. Simulation results in a horizontal channel of the DMFC agree with typical trends reported in the literature for bubbly flows. The increase in inlet flow rate is found to lead to a decrease in the gas content in the outlet of the anode channels. A case study illustrates applications of the CFD model for modelling gas evolution and current distribution in a DMFC with a parallel flow-field design. Simulation results with a improved two-phase model provide an explanation of experimental observations of a transparent DMFC with parallel channels. An improved three-dimensional CFD model includes all relevant phenomena and is valuable for gas management in a DMFC design.

Keywords: Direct methanol fuel cell; Two-phase model; Gas management; Flow-field design; Computational fluid dynamics

1. Introduction

Understanding a two-phase phenomenon is important for designing a high-performance direct methanol fuel cell (DMFC). Critical issues for improving the DMFC performance are methanol crossover, gas management on the anode side, and water management on the cathode side. Gas management is especially important in a DMFC design since the methanol electrochemical oxidation produces carbon dioxide flux on the anode side. Removing CO_2 bubbles is required to avoid blocking anode channels that may lead to limited mass transport.

A number of physicochemical phenomena take place in a DMFC, including momentum and mass transfer, electrochemical reactions, and gas–liquid flow in the anode and cathode channels. All these processes are coupled and result in a need for optimum cell design and optimum operating conditions. Thus, good understanding of these complex, interacting phenomena is essential in fuel cell design.

Researches devoted to exploring mass transfer and electrochemical reactions in DMFCs are numerous [1–11]. Scott et al. [1] examined the feasibility of using stainless-steel mesh materials as flow beds. They reported electrochemical performance and gas management characteristics with flow-beds from flow visualization studies on the anode side. Geiger et al. [2] used neutron radiography to investigate of gas-evolution patterns in anode flow-fields. It was found that gas accumulates to a large extent at the inner section of spiral channels and thereby blocks a considerable part of the active area. They noted that a spiral type of flow-field is not appropriate for the anode. Argyropoulos et al. [3] used acrylic cells to investigate visually gas evolution in an operating DMFC. They studied the effect of operating parameters and flow-bed design on gas management. It was concluded that an increase in inlet flow rate is beneficial to gas removal. Using a 5 cm^2 transparent cell, Lu and Wang [4] investigated the effects of backing pore structure and wettability on cell polarization characteristics and two-phase flow dynamics. They found that an anode backing layer of uniform pore size and high hydrophilicity is preferred for gas management in the anode. Tüber et al. [5] compared the performance of PEMFCs and DMFCs with serpentine, parallel and new fractal flow-fields. The results indicated that serpen-

* Corresponding author. Tel.: +82 2 2123 2761; fax: +82 2 312 6401.
E-mail address: ilmoon@yonsei.ac.kr (I. Moon).

0378-7753/$ – see front matter © 2006 Elsevier B.V. All rights reserved.
doi:10.1016/j.jpowsour.2006.07.071

Nomenclature

C	mass fraction (kg kg^{-1})
D	diffusion (m^2 s^{-1})
F	Faraday constant (C mol^{-1})
g	acceleration (m s^{-2})
H	membrane thickness (m)
h	channel height (m)
I	current density (A m^{-2})
I_0	exchange current density (A m^{-2})
I_e	ionic current density (A m^{-2})
j_L	capillary-diffusional flux of the liquid phase (kg m^{-2} s^{-1})
k	permeability of porous material (m^2)
K	distribution of the components
L	molar flow rate (mol s^{-1})
M	molecular weight (kg mol^{-1})
N	mass flux (kg m^{-2} s^{-1})
n	number of electrons
n_d	electro-osmotic drag coefficient
p	pressure (Pa)
s	stoichiometric coefficient
S	area (m^2)
T	temperature (K)
u	velocity (m s^{-1})
$U_0^{O_2}$	thermodynamic equilibrium potentials of oxygen reduction (V)
U_0^{MeOH}	thermodynamic equilibrium potentials of methanol oxidation (V)
v	water velocity (m s^{-1})
V_{cell}	cell voltage (V)
V_{anode}	volume of anode channels (m^3)
x	molar fraction in liquid phase (mol mol^{-1}); coordinate, (m)
y	molar fraction in gas phase (mol mol^{-1}); coordinate, (m)
z	coordinate (m)

Greek symbols

Γ_G	source of mass in gas phase (kg m^{-3} s^{-1})
α_A	charge-transfer coefficient of the anode
α_C	charge-transfer coefficient of the cathode
ε	porosity (m^3 m^{-3})
ε_G	gas content (m^3 m^{-3})
γ	local fractional vaporization; kinetic factor
η	overpotential (V)
φ	potential (V)
μ	viscosity (Pa s)
γ_c	advection correction factor
ρ	density (kg m^{-3})
σ	conductivity (m)
ψ	coefficient

Subscripts

i	component
in	inlet
out	outlet
L	liquid
G	gas
A	anode
C	cathode
eff	effective
mix	mixture
DL	diffusion layer
ref	reference value
t	total
s	interface; solid
m	membrane

Superscript

k	component (MeOH, CO_2, H_2O, O_2)

tine flow-fields give both the highest and the most stable performance.

Since it is very difficult to measure directly concentration and gas content profiles in anode channels, modelling is used to study a DMFC. Argyropoulos et al. [6] developed a model to predict the local pressure and chemical composition in the anode and cathode sides of a liquid-feed DMFC. Birgersson et al. [7] presented an isothermal, two-dimensional, liquid phase model for the conservation of mass, momentum and species in the anode channel and porous media of a DMFC. The data demonstrated the relative importance of mass transfer resistance in both the flow channel and the adjacent porous backing. Mugia et al. [8] derived a multi-component, steady-state, model based on phenomenological transport equations for the catalyst layer, diffusion layer and membrane. To understand the role of model parameters, they performed a parametric study of the model together with experimental validation. A comprehensive, two-dimensional model of two-phase flow with multi-component transport and electrochemical reactions was reported by Wang and Wang [9] for a liquid-feed DMFC, including electrodes, channels and PEM separator. Kulikovsky et al. [10] constructed a two-dimensional model for a gas-fed DMFC with a new type of current-collector. Schultz and Sundmacher [11] developed a one-dimensional, dynamic model of a DMFC based on Maxwell–Stefan mass transport equations and a Flory–Huggins activity model.

Optimum flow field design is important for improving flow patterns and gas evolution in anode channels. CFD simulation is widely used for PEMFC flow-field design [12–15]. Numerical modelling provides a better understanding of the main phenomena that govern fuel cell performance. Three-dimensional modelling is important to capture performance-limiting effects such as mass transfer and gas evolution. The conventional CFD-based model of DMFC requires experimental correlations for closure of multiphase model equations prior to numerical solution. Empirical correlations limit application of conventional sub-models for gas–liquid flow in a DMFC.

Our previous study [16] focused on a model development for gas management in the anode flow-field of a DMFC under the assumption of uniform current density. The objective of this research is to modify the three-dimensional DMFC model to predict the cell performance, concentration and potential profiles taking into account two-phase phenomena in anode channels. The improved DMFC model includes a new sub-model for interface mass transfer developed without using empirical correlations.

2. Model formulation

The model subdivides the fuel cell into seven regions, namely: anode flow channel, anode diffusion layer, anode electrocatalyst, membrane, cathode electrocatalyst, cathode diffusion layer and cathode flow channel. Each sub-model is described below.

2.1. Two-phase model for channels

The two-phase model is widely used for modelling momentum and mass transfer in gas–liquid flows [9,17–19]. Using a flow visualization technique, Yang et al. [20] developed the flow regime maps for a channel with a gas permeable sidewall. Bewer et al. [21] reported that gas–liquid flow is homogeneous during a homogeneous bubble discharge. Triplett et al. [19] compared one-dimensional simulation results with experimental data and concluded that the homogeneous model held true for bubbly flow in channels. As mentioned above, Wang and Wang [9] applied a homogeneous two-phase model for the anode channel of a DMFC. Based on flow visualization data and real application of one-dimensional and two-dimensional models, this study considers three-dimensional gas–liquid flow in anode and cathode channels with the following assumptions:

- the fuel cell is operating at a steady-state,
- the two-phase flow is isothermal, incompressible and homogeneous,
- single-phase flow in the cathode channel is isothermal without evaporation and condensation.

The model equations in Table 1 describe the distribution of velocity, the gas volume fraction and the mixture concentrations in the anode and cathode channels.

Table 1
Model equations for anode and cathode channels

Governing equations	Mathematical expression	
Continuity equation[a]	$\nabla \cdot (\rho \vec{u}) = 0$	(1)
Momentum equation[a]	$\nabla \cdot (\rho \vec{u}\vec{u}) = -\nabla p + \nabla \cdot T + \rho g$	(2)
Stress tensor[a]	$T_{ij} = \mu_{\text{eff}} \left(\frac{\partial u_i}{\partial x_j} + \frac{\partial u_j}{\partial x_i} - \frac{2}{3}\delta_{ij}\frac{\partial u_n}{\partial x_n} \right)$	(3)
Continuity equation for gas phase[a]	$\nabla \cdot (\varepsilon_{\text{G}} \rho_{\text{G}} \vec{u}_{\text{G}}) = \Gamma_{\text{G}}$	(4)
Species conservation[b]	$\nabla \cdot (\rho u C^k) = \nabla \cdot ((1-\varepsilon_{\text{G}})\rho_{\text{L}} D^k_{\text{L,eff}} \nabla C^k_{\text{L}} + \varepsilon_{\text{G}} \rho_{\text{G}} D^k_{\text{G,eff}} \nabla C^k_{\text{G}})$	(5)

[a] Sokolichin and Eigenberger [18].
[b] Wang and Wang [9].

Table 2
Model equations for diffusion layer

Governing equations	Mathematical expression	
Continuity equation[a]	$\nabla \cdot (\rho \vec{u}) = 0$	(10)
Momentum conservation[a]	$\vec{u} = -\frac{k}{\mu_{\text{L}}}(\nabla p + \rho_k g)$	(11)
Species conservation	$\nabla \cdot (\gamma_{\text{c}} \rho \vec{u} C^k) = \nabla \cdot (\rho_{\text{L}} D^k_{\text{L,eff}} \nabla C^k_{\text{L}} + \rho_{\text{G}} D^k_{\text{G,eff}} \nabla C^k_{\text{G}}) - \nabla \cdot ((C^k_{\text{L}} - C^k_{\text{G}}) j_{\text{L}})$	(12)
Ohm's law[b]	$\nabla(\sigma_{\text{c,eff}} \nabla \varphi_{\text{s}}) = 0$	(13)

[a] Wang and Wang [9].
[b] Kulikovsky et al. [10].

For single-phase gas flow in cathode channels, the gas volume fraction is $\varepsilon_{\text{G}} = 1$. The homogeneous model for channels assumes that the phases move with the same velocity. The difficulty in modelling includes multi-component mass transfer taking place across the interface. The mixture variables and properties are given by:

$$\text{density}\,(\rho) = \varepsilon_{\text{G}}\rho_{\text{G}} + (1-\varepsilon_{\text{G}})\rho_{\text{L}} \quad (6)$$

$$\text{concentration}\,(\rho C) = C_{\text{G}}\varepsilon_{\text{G}}\rho_{\text{G}} + C_{\text{L}}(1-\varepsilon_{\text{G}})\rho_{\text{L}} \quad (7)$$

$$\text{velocity}\,(\rho u) = u_{\text{G}}\varepsilon_{\text{G}}\rho_{\text{G}} + u_{\text{L}}(1-\varepsilon_{\text{G}})\rho_{\text{L}} \quad (8)$$

$$\text{viscosity}\,(\mu_{\text{eff}}) = \mu_{\text{G}}\varepsilon_{\text{G}} + \mu_{\text{L}}(1-\varepsilon_{\text{G}}) \quad (9)$$

2.2. Two-phase model for diffusion layer

According to Wang and Wang [9], a two-phase model for the porous diffusion layer is given by the model equations listed in Table 2.

Details of model variables and mixture properties are described by Wang and Wang [9].

2.3. Electrokinetics

Fluid flow and mass transfer processes occur in a DMFC in conjunction with electrochemical reactions. These processes have a significant impact on gas management and fuel cell performance. The current distribution model assumes that:

- the catalyst layer is sufficiently thin to treat it as an interface,
- isotropic porous media exists in the diffusion layer and membrane,
- negligible contact resistance,
- fully hydrated membrane,
- Tafel kinetics for irreversible reactions.

The following electrochemical reactions take place at the anode and cathode catalyst layers, respectively.

$$CH_3OH + H_2O \rightarrow CO_2 + 6H^+ + 6e^- \quad (14)$$

$$O_2 + 4H^+ + 4e^- \rightarrow 2H_2O \quad (15)$$

The current distribution model equations account for electrochemical reactions, ohmic losses and mass diffusion in the diffusion layer and catalyst layer regions [10] (Tables 3 and 4).

Table 3
Model equations for catalyst layer

Variable	Diffusion layer/membrane interface	
Solid potential	$-\sigma_{c,\mathrm{eff}}\frac{\partial\varphi_s}{\partial z} = I$	(16)
Membrane potential	$-\sigma_{m,\mathrm{eff}}\frac{\partial\varphi_s}{\partial z} = -I$	(17)
Species[a]	$-\rho_L D^k_{L,\mathrm{eff}}\frac{\partial C^k_L}{\partial z} = M^k\frac{s^k I_{\mathrm{eff}}}{n_a F}$	(18)
The anode reaction rate	$I = I^{\mathrm{MeOH}}_{0,\mathrm{ref}}\left(\frac{C^{\mathrm{MeOH}}_L}{C^{\mathrm{MeOH}}_{L,\mathrm{ref}}}\right)^{\gamma_a}\left[\exp\left(\frac{\alpha_a F}{RT}\eta\right)\right]$	(19)
The cathode reaction rate	$I = I^{O_2}_{0,\mathrm{ref}}\left(\frac{C^{O_2}_L}{C^{O_2}_{L,\mathrm{ref}}}\right)^{\gamma_c}\left[-\exp\left(-\frac{\alpha_c F}{RT}\eta\right)\right]$	(20)

[a] $I_{\mathrm{eff}} = I + I_p$.

Model Eqs. (16)–(22) with auxiliary equations and boundary conditions are taken from the original model developed by Kulikovsky et al. [10] and Wang and Wang [9]. Physicochemical properties and molecular transfer coefficients are calculated from equations cited by Wang and Wang [9].

2.4. Boundary conditions

Set conditions are required at all boundaries of the computational domains. At the inlet of both the anode and the cathode flow channels, the boundary values are prescribed from the stoichiometric flow rate and mass fractions. On all walls, a no-slip boundary condition is applied for the momentum equations and a no-flux boundary condition for the components. Boundary conditions at internal interfaces for the current model are described in detail by Mugia et al. [8] and Kulikovsky et al. [10].

2.5. Gas content in anode channels

The basic two-phase model is given by Eqs. (1)–(5). The above model equations are coupled closely, so the whole set must be solved simultaneously and iteratively. The presence of bubbles in the gas–liquid flow is reflected by the gas content ε_G and the source term Γ_G that accounts for interface mass transfer.

In accordance with the two-phase model, the gas content is found from the continuity equation (4). The source of mass in Eq. (4) by definition is:

$$\Gamma_G = M_G\frac{\delta G}{\delta V} \tag{23}$$

Carbon dioxide is produced in the anode channels by the liquid-phase electrochemical reaction (14). Gas evolution results from interface mass transfer of carbon dioxide in the anode channels. Wang and Wang [9] used a mass transfer equation with an empirical coefficient for estimating the source of the mass

$$\Gamma_G = \frac{N_{t,G}C_{G,s} + \rho_G\beta_G\Delta C_G}{h} \tag{24}$$

where $N_{t,G}$ is the total mass flux transferred from liquid to gas phase; β_G the mass transfer coefficient in the gas phase; ΔC_G the driving force of mass transfer; $C_{G,s}$ is the concentration at the interface. Estimation of the interface mass flux with the non-equilibrium model requires additional sub-models or empirical correlations for mass transfer coefficients in the gas and liquid phases. The mass transfer coefficient, in turn, is a complicated function of hydrodynamics.

As shown by Argyropoulos et al. [6] and Sundmacher and Scott [22,23], the equilibrium flash equation is suitable for computing the gas content in the anode compartment treated as a continuous stirred reactor. To define the interface flux from liquid to gas phase, it is necessary to consider the equilibrium condition in the multi-component gas–liquid flow in the anode channels. The multi-component mixture includes carbon dioxide, methanol and water. For control volume δV, we define fractional vaporization as follows:

$$\gamma = \frac{\delta G}{L + (N^{CO_2}_{\mathrm{anode}}/M^{CO_2})\,\delta S} \tag{25}$$

where δG is the molar flow rate transferred from liquid to gas phase; L the molar flow rate of liquid in a channel with volume δV; δS is the area and $\delta S = \delta V/h$.

Using the fractional vaporization Eq. (25), we suggest the following equation for estimating the source of mass

$$\Gamma_G = M_G\gamma\left(\psi + \frac{N^{CO_2}_{\mathrm{anode}}}{M^{CO_2}h}\right) \tag{26}$$

where M_G is the molecular weight of the gas phase; ψ the coefficient, $\psi = L/\delta V$. Local fractional vaporization γ is found from solving the equilibrium flash equation:

$$\sum_{i=1}^{3}\frac{(K_i - 1)C^i(M_{\mathrm{mix}}/M_i)}{(K_i - 1)\gamma + 1} = 0 \tag{27}$$

where K_i is the distribution of each component between the vapour and liquid phases, $K_i = y_i/x_i$; γ is the local fractional vaporization. The distribution of the mixture concentration C^i in the anode channels is given by the conservation equation (5). According to the electrochemical reaction (14), the mass flux of carbon dioxide is defined at diffusion layer|membrane interface as follows:

$$N^{CO_2}_{\mathrm{anode}} = M^{CO_2}\frac{1}{6}\frac{I}{F} \tag{28}$$

It should be noted that Eq. (26) corresponds to an equilibrium model of the multi-component mass transfer between the liquid and gas phases in the anode channels. Derivation of the auxiliary equation for the coefficient ψ is given in Appendix A.

Table 4
Model equations for membrane

Governing equations	Mathematical expression	
Ohm's law[b]	$\nabla(\sigma_{m,\mathrm{eff}}, \nabla\varphi_m) = 0$	(21)
Momentum conservation[a]	$\vec{u} = -\frac{k}{\mu_L}(\nabla p + \rho_k g) + \frac{n_d M}{\rho}\frac{I_e}{F}$	(22)

[a] Wang and Wang [9].
[b] Kulikovsky et al. [10].

2.6. Three-dimensional model of DMFC

The three-dimensional DMFC model is based on the conservation equations of momentum, mass and current. The coupled non-linear Eqs. (1)–(5), (10)–(13), (21) and (22) describe transfer processes in the channel, diffusion layer and membrane on both sides of the fuel cell. Current conservations are coupled with diffusion equations via the interface boundary conditions that account for the electrochemical reactions. The improved two-fluid model in the anode channels includes a new sub-model for interface mass transfer Eq. (26). Numerical simulation based on the CFD model is powerful tool for studying and predicting the effect of flow-field geometry on gas evolution, flow patterns and fuel cell performance in DMFC designs.

3. Simulation

3.1. Case study 1:1.4 cm^2 DMFC channel

In order to validate the three-dimensional CFD model with the new sub-model for interface mass transfer, this case study presents simulation results for a 1.4 cm^2 DMFC channel compared with the conventional sub-model reported by Wang and Wang [9] with the operating conditions given in Table 5.

Fig. 1 shows the development of the velocity and gas volume fraction profiles along the anode channel at different cross-sections from the inlet. The simulation results display symmetrical distributions of both the velocity and the gas volume fraction in the channel. The velocity profile corresponds to a laminar flow regime. The CFD model predicts a stable wall peak of the gas volume fraction in a horizontal channel. The distributions of velocity and gas volume fraction agree with typical trends reported in the literature for bubbly flow in channels.

Table 5
Operating conditions of 1.4 cm^2 DMFC

Channel height	2.0 mm
Channel width	2.0 mm
Number of channels	1
Cell length	7 cm
Operating temperature	80 °C
Cathode channel pressure	1 atm
Anode channel pressure	1 atm
Inlet velocity of anode channel	0.0006 m s^{-1}
Inlet methanol concentration	1 M
Inlet velocity of cathode channel	0.2 m s^{-1}
Inlet oxygen concentration	21 mol%
Inlet relative humidity at cathode	3.43 mol%

The distribution of methanol and carbon dioxide concentration along the channel are given in Fig. 2. The methanol concentration in the channel is decreased due to the electrochemical reaction (14). New sub-model Eq. (26) determines the source of the interface mass transfer in the gas–liquid flow in continuity Eq. (4).

Another point to note is that mixture properties in the diffusion layer are functions of liquid saturation. Wang and Wang [9] estimated the liquid saturation at the interface between the channel and the diffusion layer from an empirical correlation. The improved three-dimensional, two-phase model eliminates

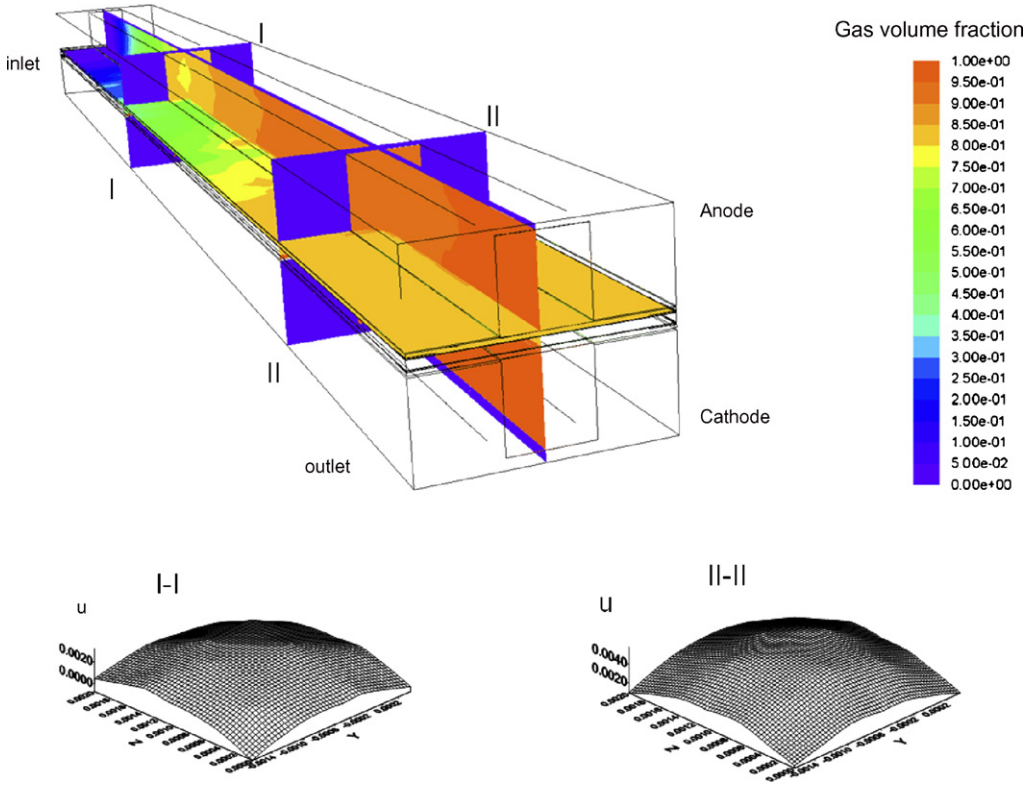

Fig. 1. Distribution of gas content (ε_G) and velocity (u) for anode channel of 1.4 cm^2 DMFC with operating conditions from Table 1. Average current density 4500 A m^{-2}.

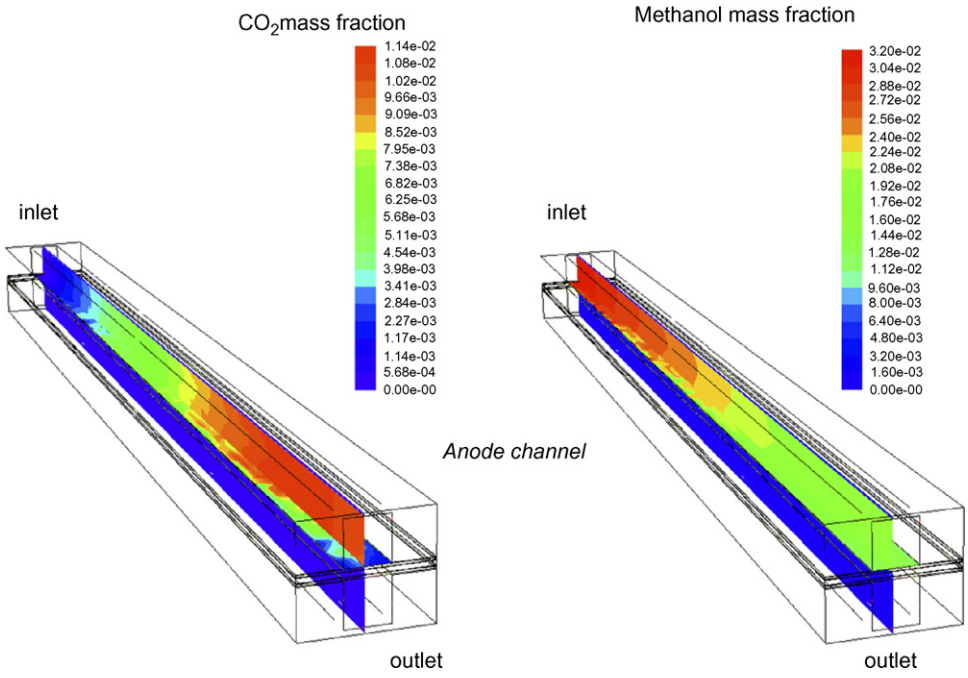

Fig. 2. Distribution of methanol (C^{MeOH}) and carbon dioxide concentration (C^{CO_2}) for anode channel of 1.4 cm^2 DMFC with operating conditions from Table 1. Average current density 4500 A m^{-2}.

using an empirical correlation for liquid saturation (or gas volume fraction) in the anode diffusion layer (Fig. 2). Non-uniform distribution of local current density in Fig. 3 at the diffusion-layer|catalyst-layer interface results from non-uniform supply of reactant along the anode channel and mass transfer in the diffusion porous layer.

Fig. 4 shows the fuel cell slice with the predicted distribution of overpotential ($\eta = \varphi_s - \varphi_m$) at $x = 0.03$ m from the channel inlet. The predictions reveal a complicated interaction between the current-collector and the porous conductor. Strong peaks of electron current and gradient of potential occur near the edges of the current-collector on both sides of the fuel cell. These edges collect current under anode and cathode channels, respectively. The peak current is about 10 times higher than the mean current density. Similar results for a porous diffusion layer were reported by Kulikovsky et al. [10] from a two-dimensional model for a gas-fed DMFC.

Fig. 5 provides a comparison of the velocity, concentration and gas content profiles along the anode channel calculated by the new model Eq. (26) and profiles corresponding to the conventional sub-model Eq. (24) with empirical mass transfer coefficients. The empirical correlation has been developed for mass transfer from bubble to liquid by Taylor flow in the circular capillary tube of a monolithic catalyst reactor [24]. It should

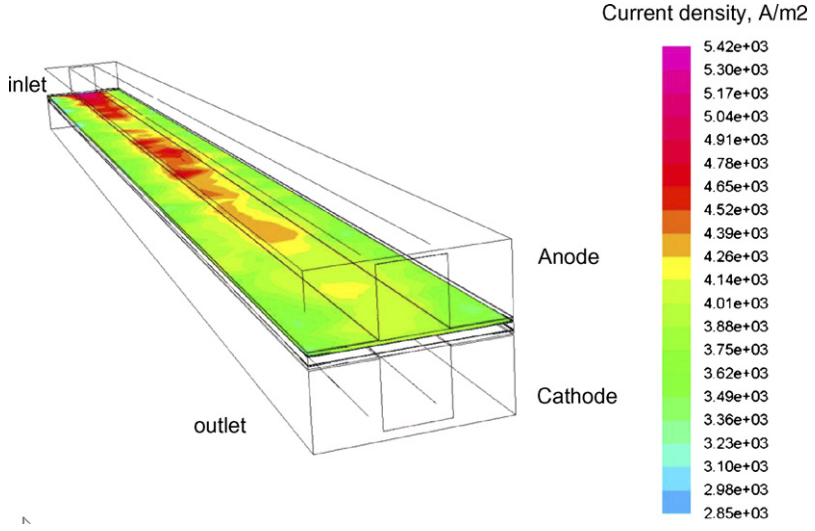

Fig. 3. Distribution of local electron current density (I) at diffusion-layer|membrane interface for 1.4 cm^2 DMFC with operating conditions from Table 1. Average current density 4500 A m^{-2}.

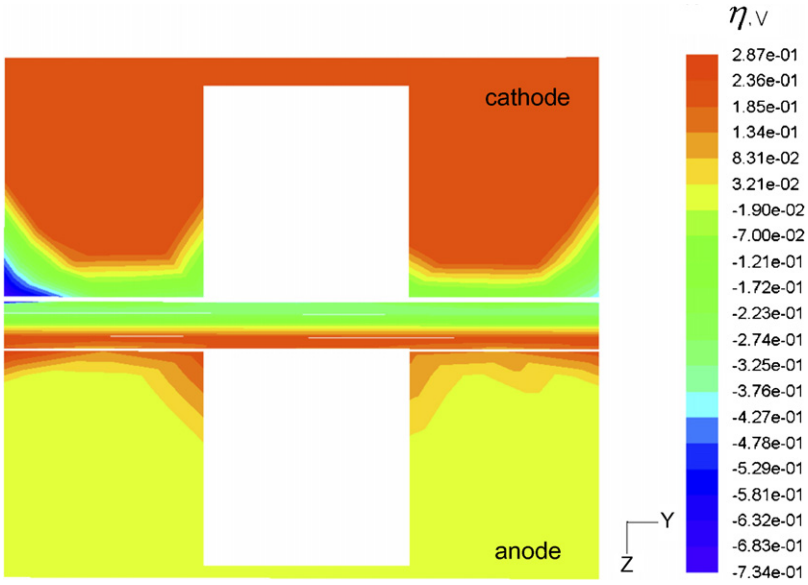

Fig. 4. Fuel cell cross-section with distribution of overpotential (η) at $x = 0.03$ m from the inlet. Horizontal channel of 1.4 cm^2 DMFC with operating conditions in Table 1. Average current density 4500 A m^{-2}.

be noted that gas phase evaluation with mass transfer equations corresponds to a non-equilibrium model of transfer processes in the anode channels. The new sub-model Eq. (26) without empirical coefficients is in accord with an equilibrium model of the mass transfer process in gas–liquid flow.

Simulation results in Fig. 5 quantitatively agree with the two-dimensional simulation data reported by Wang and Wang [9]. The void fraction in the anode channel increases along the flow direction from 0% at the inlet to 90% at the outlet. The velocity increases along the flow direction due to the volume expansion of the two-phase mixture. Fig. 6 presents simulation outcomes with the predicted dependence of the outlet gas content on the inlet flow rate for the channel. As appears from the above three-dimensional CFD model, an increase in the inlet flow rate leads to a decrease in the gas content at the outlet section.

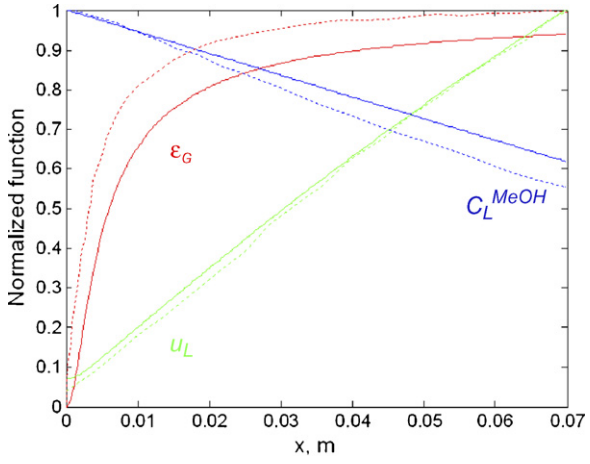

Fig. 5. Comparison of gas–liquid characteristics predicted by conventional and new sub-model for interface mass transfer. Case study of 1.4 cm^2 DMFC. (Solid lines) Averaged three-dimensional CFD model with new sub-model Eq. (26). (Dashed lines) One-dimensional model with conventional sub-model Eq. (24) reported by Wang and Wang [9]. Average current density 4500 A m^{-2}.

Gas content and channel blocking can be reduced significantly at higher liquid flow rates. The model predictions agree with the visualization study reported by Scott et al. [1] for a transparent DMFC with parallel channels. These findings are important for optimizing the operation of DMFCs.

3.2. Case study 2: DMFC with parallel flow-field

For additional testing of the proposed model, simulation results for a DMFC are compared with experimental data obtained by Lu and Wang [4] with the operating conditions given in Table 6. They reported results for both anode and cathode from simultaneous two-phase flow visualization with a transparent 5 cm^2 DMFC.

Taking operation data as input, we have applied the proposed model for the simulation of a DMFC with parallel channels. The distribution of the calculated velocity and gas content in the

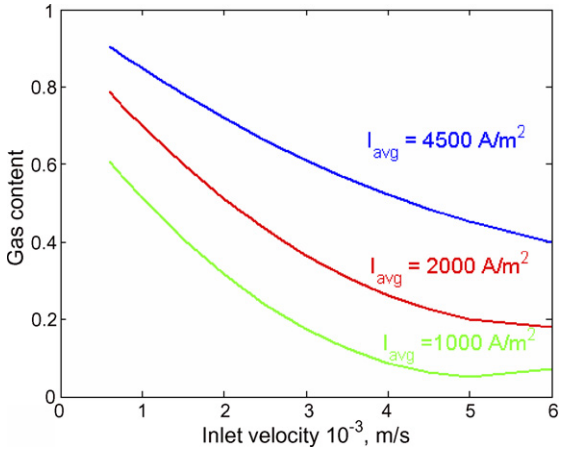

Fig. 6. Dependence of gas content on inlet flow rate of methanol solution. Case study of 1.4 cm^2 DMFC.

Table 6
Operating conditions of 5 cm^2 DMFC

Channel height	1.5 mm
Channel width	1.92 mm
Number of channels	8
Cell effective area	5.0 cm^2
Operating temperature	85 °C
Cathode channel pressure	15 psig
Anode channel pressure	0 psig
Inlet methanol stream flow rate	20.8 ml min^{-1}
Inlet methanol concentration	2 M
Inlet air stream flow rate	700.0 ml min^{-1}
Inlet oxygen concentration	21 mol%

anode channels are given in Fig. 7. The CFD model predicts a highly non-uniform velocity field in the parallel channels and shows high values at the lateral channels and a nearly stagnant zone in the central region. Simulation results agree with the observation of bubble dynamics in the channels. The mean gas content, $\bar{\varepsilon}_G$, along anode channels computed from images of bubbles reported by Lu and Wang [4] is between 0 and 22%.

The distribution of local electron current shown in Fig. 8 reveals a non-uniform supply of reactants through the diffusion-layer|catalyst-layer interface for a DMFC with parallel channels.

The interaction between the transfer processes in a DMFC with parallel flow-field are presented in Figs. 7–9. Non-uniform distribution of flow, gas volume fraction, species and current density profiles in parallel channels confirms the importance of the flow-field in a DMFC design.

The calculated polarization curve in Fig. 10 agrees well with the experimental data for a 5 cm^2 DMFC reported by Lu and Wang [4]. According to the operating conditions in Table 2, the inlet methanol solution is saturated with dissolved CO_2.

4. Results and discussion

Gas management depends on various parameters, e.g., material properties, cell design and operating conditions. Channel blocking restricts the supply of reactants to the catalyst layer and hence leads to deterioration in cell electrical performance. The efficient removal of carbon dioxide is an important factor in DMFC design. The main objective of gas management is to determine a DMFC design and operating conditions so as to provide uniform distribution of liquid without gas accumulation in the channels. A two-fluid model is suitable for gas management in a DMFC. The conventional two-fluid model uses a non-equilibrium sub-model with empirical coefficients

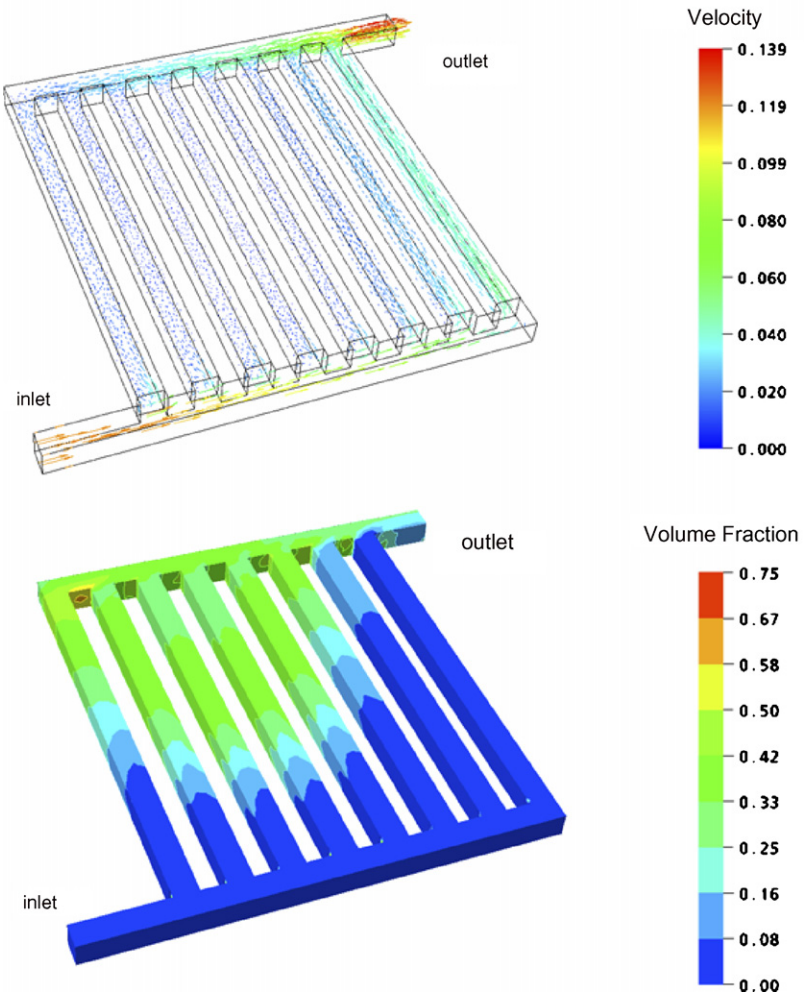

Fig. 7. Distribution of gas content (ε_G) and velocity (u) for 5 cm^2 DMFC with operating conditions in Table 2. Average current density 2000 A m^{-2}.

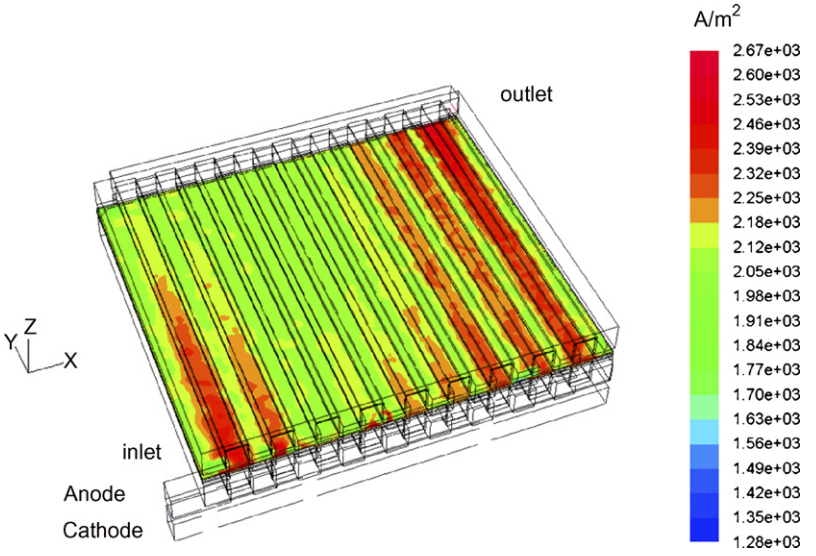

Fig. 8. Distribution of electron current density at diffusion-layer|membrane interface for 5 cm^2 DMFC with operating conditions in Table 2. Average current density 2000 A m^{-2}.

for interface mass transfer. Wang and Wang [9] showed the application of a homogeneous two-fluid model for a DMFC with a conventional sub-model of interface mass transfer with empirical correlations. We suggest a new equilibrium sub-model for estimating the interface mass transfer in anode channels. In contrast to Wang and Wang [9], we use the improved CFD-based two-phase model with the new sub-model for interface mass transfer without using empirical correlations. This study shows the application of the three-dimensional CFD model for exploring gas evolution in a DMFC with parallel channels. The above flow-field simulations provide a good illustration of the capability of the model.

The design of a DMFC requires an understanding of processes such as mass, momentum transport, electrochemical reactions and charge balance that are taking place inside the cell. The CFD model predicts a stable wall peak of the gas volume fraction in the horizontal channel. The calculated distribution of velocity and gas volume fraction agrees with typical trends reported in the literature for bubbly flow in channels. The calculated three-dimensional profiles in a 1.4 cm^2 DMFC channel display a strongly non-uniform distribution of electronic current in the collector and the diffusion layer. The current is concentrated on the edges of the collector. A CFD model of a DMFC is a valuable tool for developing a modified collector to ensure uniform potential and current distribution.

As shown in this study, the flow geometry of the anode side has an important impact on gas evolution. Simulation results reveal that a parallel flow-field is not suitable for gas management in a DMFC. Flow maldistribution also occurs in parallel channels with single-phase flow. Barreras et al. [25]

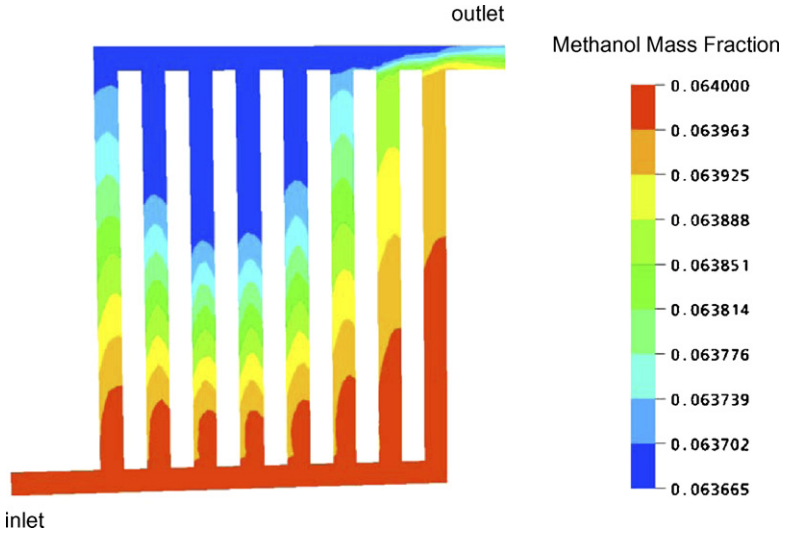

Fig. 9. Distribution of methanol concentration at $z = h/2$ cross-section of anode channels for 5 cm^2 DMFC with operating conditions in Table 2. Average current density 2000 A m^{-2}.

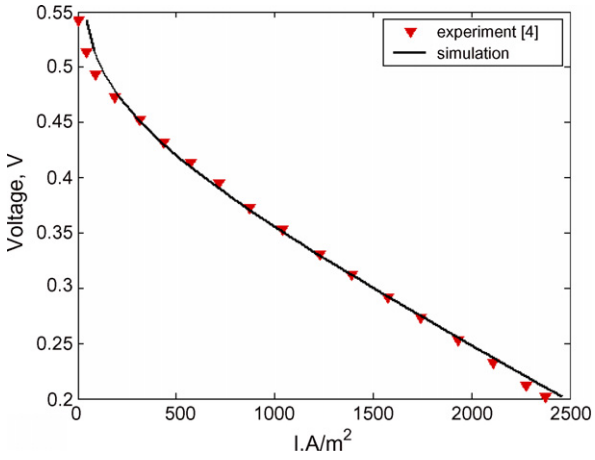

Fig. 10. Comparison of numerically predicted polarization curve with experimental data for 5 cm^2 DMFC. (Points) Experimental data reported by Lu and Wang [4]. (Solid line) Simulation results with three-dimensional CFD model.

have performed an experimental and numerical research of the single-phase flow distribution in a bipolar plate with a parallel flow-field. They also concluded that the single-phase flow preferentially moves through the lateral channels and results in an inappropriate distribution on the electrode surfaces.

It should be noted that the simulation results and the main conclusions qualitatively agree with experimental observations for a transparent DMFCs available in literature. One of the advantages of computational modelling is the ability to evaluate innovative designs [16,26]. The model developed here is useful for the basic understanding of three-dimensional transport and electrochemical phenomenon in DMFCs, and for the optimization of cell design and operating conditions.

5. Conclusions

A CFD-based two-phase model has been developed for a DMFC. The improved two-phase model includes a new submodel for interface transfer without using any empirical correlation for gas–liquid flow in the anode channels. Simulation results agree with typical trends for bubbly flows in channels. It is found that flow-field design has a very significant influence on to the performance and gas management of DMFCs. The CFD model is validated against the polarization curve for a 5 cm^2 DMFC. An increase in inlet methanol solution flow rate is found to lead to a decrease in the total outlet gas content on the anode side. Interaction between the current collector and the diffusion layer leads to a complex distribution of current and potential in fuel cell. Computational results furnish explanations of the observed flow in transparent DMFCs, as reported by other workers. The proposed model is valuable in CFD-based DMFC design.

Acknowledgements

This work was supported by a grant from the Korean Federation of Science and Technology Societies.

Appendix A

Assuming the coefficient ψ is constant, we can evaluate it from total mass balance for gas phase

$$G_{\text{in}} - G_{\text{out}} = \bar{\Gamma}_{\text{G}} V_{\text{anode}} \tag{A.1}$$

where G_{in} is the gas flow rate at inlet section; $G_{\text{in}} = 0$; G_{out} the gas flow rate at the outlet section; V_{anode} is the volume of anode channels. The gas flow rate at the outlet section is

$$G_{\text{out}} = u_{\text{G,out}} \rho_{\text{G}} \varepsilon_{\text{G}}^{\text{out}} S_{\text{out}} \tag{A.2}$$

where S_{out} is the area of the stream outlet section; $u_{\text{G,out}}$ the velocity of gas at section S_{out}; ε^{out} is the gas content in the two-phase stream at section S_{out}. The gas content at the outlet section of anode channel is calculated using:

$$\varepsilon_{\text{G}}^{\text{out}} = \frac{\gamma^{\text{out}} \rho_{\text{mol,L}}}{\gamma^{\text{out}} \rho_{\text{mol,L}} + (1 - \gamma^{\text{out}}) \rho_{\text{mol,G}}} \tag{A.3}$$

The mean source of gas is:

$$\bar{\Gamma}_{\text{G}} = M_{\text{G}} \bar{\gamma} \left(\psi + \frac{\bar{N}_{\text{anode}}^{\text{CO}_2}}{M^{\text{CO}_2} h} \right) \tag{A.4}$$

where M_{G} is the molecular weight of gas phase; ψ the coefficient, $\psi = L/\delta V$; $\bar{\gamma}$ the mean fractional vaporization, $\bar{\gamma} = (1/V_{\text{anode}}) \int \gamma \, \text{d}V$. The mean mass flux of the carbon dioxide component in the anode channel is:

$$\bar{N}_{\text{anode}}^{\text{CO}_2} = M^{\text{CO}_2} \frac{1}{6} \frac{I_{\text{avg}}}{F} \tag{A.5}$$

The fractional vaporization γ^{out} at the outlet section of the anode channel is given by:

$$\sum_{i=1}^{3} \frac{(K_i - 1) C_i^{\text{out}} (M_{\text{mix}}/M_i)}{(K_i - 1)\gamma^{\text{out}} + 1} = 0 \tag{A.6}$$

where component molar fraction at the outlet section is evaluated from mass balance.

Finally, solving Eqs. (A.4) and (A.1) for ψ we have [16,26]:

$$\psi = \frac{G_{\text{in}} - G_{\text{out}}}{V_{\text{anode}} M_{\text{G}} \bar{\gamma}} - \frac{\bar{N}_{\text{anode}}^{\text{CO}_2}}{M^{\text{CO}_2} h} \tag{A.7}$$

References

[1] K. Scott, P. Argyropoulos, P. Yiannopoulos, W.M. Taama, J. Appl. Electrochem. 31 (2001) 823–832.
[2] A. Geiger, E. Lehmann, P. Vontobel, G.G. Scherer (Eds.), Scientific Report 2000, vol. V, Switzerland, pp. 86–87 (http://www1.psi.ch/).
[3] P. Argyropoulos, K. Scott, W.M. Taama, J. Appl. Electrochem. 29 (1999) 661–669.
[4] G.Q. Lu, C.Y. Wang, J. Power Sources 134 (2004) 33–40.
[5] K. Tüber, A. Oedegaard, M. Hermann, C. Hebling, J. Power Sources 131 (2004) 175–181.
[6] P. Argyropoulos, K. Scott, W.M. Taama, Chem. Eng. J. 78 (2000) 29–41.
[7] E. Birgersson, J. Nordlund, H. Ekström, M. Vynnycky, G. Lindberghb, J. Electrochem. Soc. 150 (2003) A1368–A1376.
[8] G. Mugia, L. Pisani, A.K. Shukla, K. Scott, J. Electrochem. Soc. 150 (2003) A1231–A1245.
[9] Z.H. Wang, C.Y. Wang, J. Electrochem. Soc. 150 (2003) A508–A519.

[10] A.A. Kulikovsky, J. Divisek, A.A. Kornyshev, J. Electrochem. Soc. 147 (2000) 953–959.
[11] Th. Schultz, K. Sundmacher, J. Power Sources 145 (2005) 435–462.
[12] D. Cheddie, N. Munroe, J. Power Sources 147 (2005) 72–84.
[13] E. Birgersson, M. Noponen, M. Vynnyckya, J. Electrochem. Soc. 152 (2005) A1021–A1034.
[14] B.R. Sivertsen, N. Djilali, J. Power Sources 141 (2005) 65–78.
[15] Ph.Th. Nguyen, T. Berning, N. Djilali, J. Power Sources 130 (2004) 149–157.
[16] V.A. Danilov, J. Lim, I. Moon, K. Choi. Korean J. Chem. Eng. 23 (2006), in press.
[17] D. Drew, Ann. Rev. Fluid Mech. 15 (1983) 261–291.
[18] A. Sokolichin, G. Eigenberger, A. Lapin, A. Lübbert, Chem. Eng. Sci. 52 (1997) 611–626.
[19] K.A. Triplett, S.M. Ghiaasiaan, S.I. Abdel-Khalik, A. LeMouel, B.N. McCord, Int. J. Multiphase Flow 25 (1999) 395–410.
[20] H. Yang, T.S. Zhao, P. Cheng, Int. J. Heat Mass Transfer 47 (2004) 5725–5739.
[21] T. Bewer, T. Beckmann, H. Dohle, J. Mergel, D. Stolten, J. Power Sources 125 (2004) 1–9.
[22] K. Scott, P. Argyropoulos, J. Electroanal. Chem. 567 (2004) 103–109.
[23] K. Sundmacher, K. Scott. Chem. Eng. Sci. 54 (1999) 2927–2936.
[24] S. Irandous, B. Andersen, Comput. Chem. Eng. 13 (1989) 519–526.
[25] F. Barreras, A. Lozano, L. Valiño, C. Marín, A. Pascau, J. Power Sources 144 (2005) 54–66.
[26] V.A. Danilov, J. Lim, I. Moon, K.H. Choi, AIChE Annual Meeting October 30–November 4, Cincinnati, OH, 2005.